Low index contrast heterostructure photonic crystal cavities with high quality factors and vertical radiation coupling

Xiaochen Ge, Momchil Minkov, Shanhui Fan, Xiuling Li, and Weidong Zhou

Citation: Appl. Phys. Lett. **112**, 141105 (2018); doi: 10.1063/1.5026433
View online: https://doi.org/10.1063/1.5026433
View Table of Contents: http://aip.scitation.org/toc/apl/112/14
Published by the American Institute of Physics

Low index contrast heterostructure photonic crystal cavities with high quality factors and vertical radiation coupling

Xiaochen Ge,[1] Momchil Minkov,[2] Shanhui Fan,[2,a)] Xiuling Li,[3] and Weidong Zhou[1,a)]
[1]*Department of Electrical Engineering, University of Texas at Arlington, Arlington, Texas 76019, USA*
[2]*Department of Electrical Engineering, Stanford University, Stanford, California 94305, USA*
[3]*Department of Electrical and Computer Engineering, University of Illinois Urbana-Champaign, Urbana, Illinois 61801, USA*

(Received 19 February 2018; accepted 26 March 2018; published online 3 April 2018)

We report here design and experimental demonstration of heterostructure photonic crystal cavities resonating near the Γ point with simultaneous strong lateral confinement and highly directional vertical radiation patterns. The lateral confinement is provided by a mode gap originating from a gradual modulation of the hole radii. High quality factor resonance is realized with a low index contrast between silicon nitride and quartz. The near surface-normal directional emission is preserved when the size of the core region is scaled down. The influence of the cavity size parameters on the resonant modes is also investigated theoretically and experimentally. *Published by AIP Publishing.* https://doi.org/10.1063/1.5026433

Enabled by the slow light phenomenon at the band edge, photonic crystal (PhC) heterostructure cavities have been widely used for achieving lateral confinement within two-dimensional photonic crystal slabs. Heterostructure cavities can be formed by either modulating the filling factors[1–4] or embedding different types of lattices.[5] Currently, most reported heterostructure PhC cavities are based on the band edge modes below the light cone, where the light is vertically confined within the dielectric slab by total internal reflection. However, the emission from such cavities is the strongest at large angles from the surface normal direction. It is challenging to apply these heterostructure cavities for free-space laser applications since the brightness is limited by the far field radiation beam quality. For these cavities, since the emission is dominantly in-plane through the edge of the slab, a high numerical aperture (NA) lens would generally be required for efficiently collecting the emission in large angles.

Complementary to efforts for improving the radiation pattern and out of plane coupling efficiency of the modes below the light cone,[6–9] there is also an increasing interest on the PhC modes above the line cone.[10] In particular, at the Γ point, the radiation is intrinsically surface normal, and an extremely high quality factor (Q) can be made possible using the concept of the bound state in continuum[11] (BIC). The photonic crystal surface-emitting laser (PCSEL)[12–15] based on such principles is a promising platform for large area high power and high beam quality applications.[16] On the other hand, there is also demand on scaling down the active region to achieve lasers with low threshold, high energy efficiency, and high modulation speed.[17–19] Efforts were devoted to achieving lateral confinement in defect free PhC structures such as using distributed Bragg reflectors[17,20] at the edges of the PhC lattices, using rod type PhC unit cells,[19] which have a high index contrast with the surrounding air, exploring the non-symmetry-protected BIC in higher order bands.[21] There are also theoretical investigations on heterostructures in square lattice rods[3] and honeycomb lattice holes.[4]

In this work, we show that, both theoretically and experimentally, without a complete photonic bandgap, it is still possible to achieve efficient lateral confinement and high Q within a hexagonal lattice by a heterostructure formed by tuning the hole radii. The fact that the starting modes are above the light cone means that the requirement of refractive index contrast can be relaxed as there is no need for opening a complete photonic bandgap, which is beneficial for visible wavelengths where a high refractive index material is limited. We also discuss the effect of the size scaling on the far field radiation and resonant modes.

Silicon nitride is chosen as the material for demonstrating the concept as it is transparent in both visible and near infrared regions, and it is furthermore compatible with the complementary metal oxide semiconductor (CMOS) technology and widely used in integrated photonics. Figure 1(a) shows a sketch of the cavity in which a silicon nitride ($n = 1.97$) film on quartz ($n = 1.53$) is considered. The PhC is formed by a hexagonal lattice of air holes with period $a = 460$ nm, while the thickness of the silicon nitride slab is $h = 160$ nm. The heterostructure cavity is composed of three regions, denoted as the core region, the transitional region, and the cladding region from the center to the edge of the PhC lattice with decreasing hole radii ($R_{core} = 0.24a$, $R_{trans} = 0.22a$, and $R_{clad} = 0.20a$ for the rest of the presented work). The sizes of those regions, defined as the number of layers of air holes in each region, are noted as N_{core}, N_{trans}, and N_{clad}, respectively, as shown in Fig. 1(b). The simulated TE-like band diagrams of the PhC in each region near Γ are plotted in Fig. 1(c). For an infinite uniform hexagonal PhC lattice, the mode at the Γ point on top of the second band is a symmetry protected BIC ("dark mode") which does not couple to the free space. Tuning the radius of the holes would slightly shift the frequency of the band while keeping the property of the dark mode at Γ intact. By choosing the radius in the core region larger than that in the other regions of the cavity, the mode

a)Authors to whom correspondence should be addressed: shanhui@stanford.edu and wzhou@uta.edu

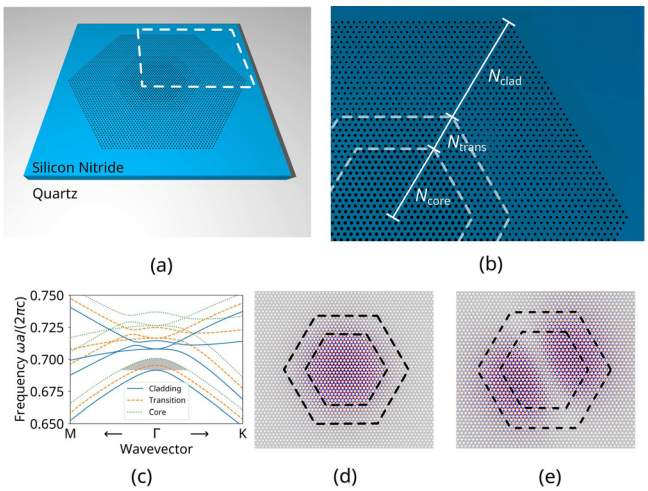

FIG. 1. Design of the heterostructure PhC cavity. (a) Sketch of the silicon nitride PhC cavity on a quartz substrate. (b) Zoom-in view of the top right corner in (a), showing the separation between each cavity region and the definition of N_{core}, N_{trans}, and N_{clad}. (c) Simulated band diagram of the PhC in different regions around the Γ point. The shaded area is the mode gap. (d) and (e) Simulated field distribution H_z of the fundamental and second order cavity modes at the center of the slab overlaid on the cavity structure ($N_{core} = 12$, $N_{trans} = 6$, and $N_{clad} = 40$). The dashed lines indicate the separation between regions.

near the Γ point in the core region would have a higher frequency, which prohibits it from coupling with the similar modes in the cladding region. In other words, a mode gap near Γ would be formed between the modes in the core and cladding regions, as shown in the shaded area. Although the PhC under consideration does not support a full in-plane bandgap in this wavelength range, the coupling between the core modes in the mode gap to the higher order cladding modes with the same frequency is expected to be small owing to the mismatch of the effective indices and mode patterns. Therefore, in this heterostructure configuration, the cavity mode can be confined vertically in the slab by the high Q pseudo-BIC and laterally in the core region by the mode gap.

We simulated the resonant modes of the heterostructure PhC cavity using the finite-difference time domain (FDTD) method.[22] The resolution of the simulation is 20 grids per lattice constant. Multiple resonant modes are supported by the cavity due to the lateral confinement. The magnetic field H_z distribution of the fundamental and second order cavity modes is plotted in Figs. 1(d) and 1(e), respectively. In the rest of the work, we will focus on the properties of the fundamental mode, which is better confined both laterally and vertically owing to the strength of the mode gap and the proximity to Γ.

Encouraged by the simulation results, we fabricated the heterostructure PhC samples. A silicon nitride film of 160 nm thickness was deposited on a quartz substrate by low pressure chemical vapor deposition (LPCVD). ZEP520A resist was spun-coated, and the PhC pattern was defined by electron beam lithography. The pattern was then transferred to the silicon nitride layer using inductively coupled plasma reactive ion etching with a gas combination of SF_6, CHF_3, and He. After dissolving the resist, the sample was cleaned by an oxygen plasma descum process to remove the residue. Figure 2(a) shows the scanning electron microscopy (SEM) image of a fabricated cavity.

Silicon nitride has a broadband fluorescence introduced by the defects or impurities during deposition. This intrinsic fluorescence can be used as an internal light source to characterize cavity resonances.[23] We characterized the cavities using a home-built micro-photoluminescence (μ-PL) system. Light from a 445 nm laser was focused onto the center of the core region using an Olympus 10×, 0.25 NA objective lens. The PL signal was collected using the same lens and directed to a monochromator (Horiba iHR-550), dispersed using a 1200 g/mm grating and detected using a cooled CCD camera (Horiba Synapse). The PL spectrum of a heterostructure PhC is plotted in Fig. 2(b), showing a sharp resonance peak corresponding to the high Q fundamental mode of the cavity. A series of high order transverse modes are also visible in the spectrum. Since the band edge around Γ, in which the cavity modes are located, is at the top of the band, the high order modes, which have $\mathbf{k}$ further away from Γ, have longer wavelengths than the fundamental mode. The resonance peak of the fundamental mode is fitted with a Lorentzian function and plotted in Fig. 2(c). With the confidence interval in 3 standard deviations, the fitted wavelength is $\lambda = 659.0014 \pm 6.5 \times 10^{-4}$ nm and the full width half maximum (FWHM) linewidth is $\Delta\lambda = 0.0435 \pm 2.6 \times 10^{-3}$ nm, corresponding to $Q \approx 15\,000$. We believe that the measured linewidth is limited by the spectral resolution of our instrument as there are only two pixels located at the resonant peak.

We now consider the size scaling properties of the heterostructure PhC design with respect to far field radiation, the wavelength, and the Q factor. As most of the cavity mode is concentrated in the core region, the size parameter N_{core} is expected to have the most significant impact. In Fig. 3, we plot the far field electric field intensity computed through a near-to-far field transformation[24] for three cavities with core sizes $N_{core} = 4$, $N_{core} = 12$, and $N_{core} = 20$, while the other two parameters are fixed to be $N_{trans} = 6$ and $N_{clad} = 40$ for all three cases. As expected from the fact that the heterostructure cavity is based on a mode at the Γ point of the underlying regular crystal, the emission is strongly localized around the vertical direction. We can quantify the efficiency η within a given collection angle θ_c as

$$\eta(\theta_c) = \frac{\int_{\Omega(\theta_c)} |\mathbf{E}_{FF}(\theta,\phi)|^2 \sin\theta \, d\theta d\phi}{\int_{\Omega(90^\circ)} |\mathbf{E}_{FF}(\theta,\phi)|^2 \sin\theta \, d\theta d\phi}, \quad (1)$$

where $\Omega(\theta)$ is the solid angle from 0 to θ_c and $\mathbf{E}_{FF}$ is the far-field electric field. For $\theta_c = 10^\circ$, corresponding to a

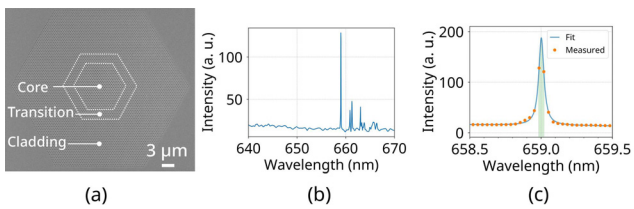

FIG. 2. Experimental demonstration of the heterostructure cavity. (a) SEM image of a representative cavity. (b) Measured photoluminescence spectrum of a fabricated sample ($N_{core} = 20$, $N_{trans} = 6$, and $N_{clad} = 40$). (c) Lorentzian fitting of the fundamental cavity mode. The 0.0435 nm FWHM is shaded in green.

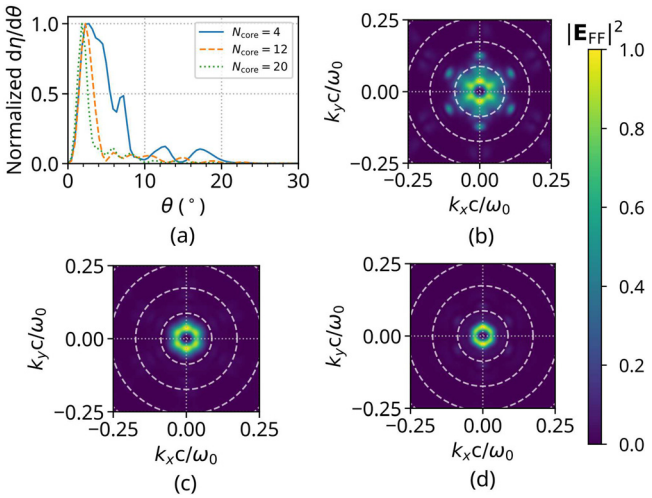

FIG. 3. Far field radiation of the fundamental cavity mode. (a) Angle dependent radiation profile. (b)–(d) Far field electric field intensity distributions versus **k** with N_{core} values of 4, 12, and 20, respectively. The white dashed lines show the emission angle θ in steps of 5°.

numerical aperture of 0.17, the efficiency η is 0.86, 0.88, and 0.94 for the three modes, respectively, in Figs. 3(b)–3(d). Since the far field is proportional to the Fourier transform of the near field, the spot size decreases with the increasing core size, showing a trend similar to that of the coupled PhC cavity system.[9] The high η means that nearly all of the emitted light can be easily collected through a small numerical aperture in the vertical direction, as shown in Fig. 3(a). This is a significant advantage in terms of extraction efficiency when compared to similar systems which are however not based on a Γ-point mode.[1,2,5] Engineering a Gaussian-like beam is desirable in general free-space applications.[16] In the presented design, the confined mode is formed by the PhC band modes close to the Γ-point, and the fact that the starting band has a dark mode at Γ results in the doughnut-shape far-field distribution. However, we expect that a similar approach can be applied starting from a band with a mode with a high yet finite Q at Γ, such that a maximum in the normal direction in the far field can be achieved.

We fabricated a series of heterostructure PhCs with different size parameters to investigate the influence of size on the fundamental cavity mode experimentally. The results are summarized in Fig. 4. The difference between the simulated and measured wavelengths in Figs. 4(a) and 4(b) is from the systematic uncertainty in the radius and slab thickness. In Figs. 4(a) and 4(d), the cavity under consideration has varying N_{core} and fixed $N_{trans} = 6$ and $N_{clad} = 40$. It can be seen that with the increase in N_{core}, the resonant mode would approach the Γ point located at the band top. The theoretical Q increases monotonically, and one may infer that as N_{core} approaches infinity, the mode would become a true BIC with a diverging Q. Experimentally, the measured Q factor is limited by the instrument, saturating at larger N_{core}. To investigate the influence of N_{clad}, we have chosen the set of parameters with $N_{core} = 12$ and $N_{trans} = 6$ in Figs. 4(b) and 4(e) as the core size would not lead to instrument limited Q. Figure 4(b) shows that N_{clad} has minimum influence on the resonant wavelength, which can be understood as the simulated field distribution in Fig. 1(d) has little overlap with the cladding region. Moreover, the Q factor saturates for both theoretical and experimental cases, which indicates that the limiting factor of the cavity leakage changes from $Q_{\parallel}$ to $Q_{\perp}$ with increasing N_{clad}. In surface emitting lasers, the suppression of lateral leakage would lead to an improved energy extraction in the out-of-plane direction. The difference between theoretical and experimental Q factors is likely due to the imperfections in fabrication. In Figures 4(c) and 4(f), we plotted the measured N_{core} dependent wavelength and Q with N_{trans} values of 2, 4, and 6, respectively, while the cladding size was kept constant at 40. Similar to the case of N_{clad}, N_{trans} also has minimum impact on the wavelength. On the other hand, a larger N_{trans}, which means a gentler transition in the real space, leads to a narrower spread of the field in the **k** space, resulting in a higher Q.

By incorporating a heterostructure in the PhC lattice, a mode gap near the Γ point would provide lateral confinement for the surface emitting mode above the light cone. The presented cavity design has near surface normal far field

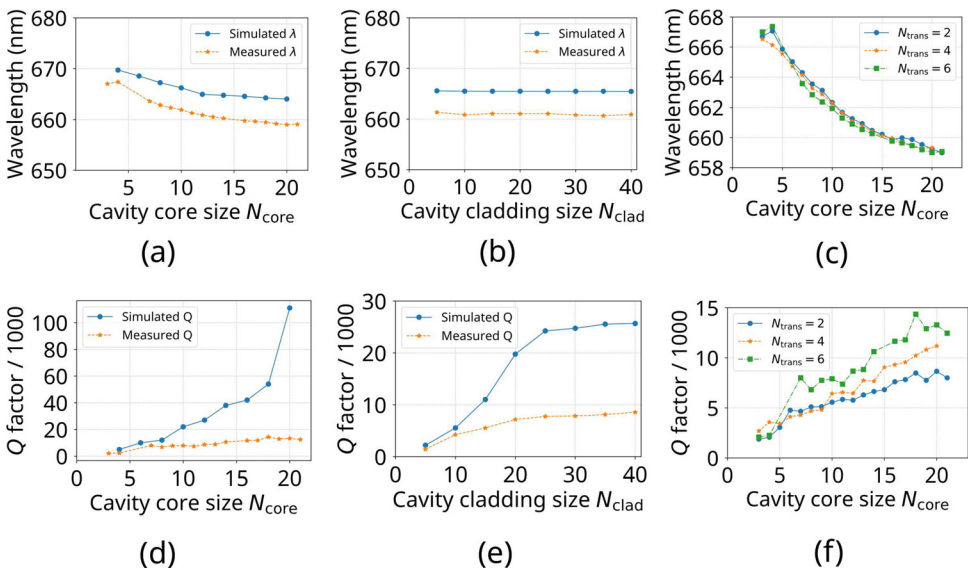

FIG. 4. Size scaling of the resonant wavelength and Q factor. (a) and (d) Simulated and measured wavelength and Q depending on N_{core}. (b) and (e) Simulated and measured wavelength and Q depending on N_{clad}. (c) and (f) Measured dependence of the wavelength and Q on N_{core} for several values of N_{trans}.

radiation even with scaling down of the cavity size. Compared to defect free PhCs used in PCSELs, a high Q factor and less in-plane leakage can be realized in a design with a more compact active region. We believe that the presented design can serve as a platform for high efficiency, low threshold surface emitting lasers.

The presented work was supported by Air Force Office of Scientific Research Grant No. FA9550-16-1-0010. M.M. acknowledges the funding from the Swiss National Science Foundation Project No. P2ELP2_165174.

[1]S.-H. Kwon, S.-H. Kim, S.-K. Kim, Y.-H. Lee, and S.-B. Kim, Opt. Express **12**, 5356 (2004).
[2]F. Bordas, M. Steel, C. Seassal, and A. Rahmani, Opt. Express **15**, 10890 (2007).
[3]L. Ferrier, P. Rojo-Romeo, E. Drouard, X. Letartre, and P. Viktorovitch, Opt. Express **16**, 3136 (2008).
[4]P. Nedel, X. Letartre, C. Seassal, A. Auffèves, L. Ferrier, E. Drouard, A. Rahmani, and P. Viktorovitch, Opt. Express **19**, 5014 (2011).
[5]A. V. Giannopoulos, Y.-J. Li, C. M. Long, J.-M. Jin, and K. D. Choquette, Opt. Express **17**, 5379 (2009).
[6]S. Combrié, P. Colman, A. De Rossi, and T. Mei, Phys. Rev. B **82**, 075120 (2010).
[7]M. Minkov, V. Savona, and D. Gerace, Appl. Phys. Lett. **111**, 131104 (2017).
[8]J. Huang, S.-H. Kim, J. Gardner, P. Regreny, C. Seassal, P. Aitor Postigo, and A. Scherer, Appl. Phys. Lett. **99**, 091110 (2011).
[9]S.-H. Kwon, Appl. Phys. Express **3**, 112001 (2010).
[10]S. Fan and J. Joannopoulos, Phys. Rev. B **65**, 235112 (2002).
[11]J. Lee, B. Zhen, S.-L. Chua, W. Qiu, J. D. Joannopoulos, M. Soljačić, and O. Shapira, Phys. Rev. Lett. **109**, 067401 (2012).
[12]S. Noda, K. Kitamura, T. Okino, D. Yasuda, and Y. Tanaka, IEEE J. Sel. Top. Quantum Electron. **23**, 1 (2017).
[13]D. Zhao, S. Liu, H. Yang, Z. Ma, C. Reuterskiöld-Hedlund, M. Hammar, and W. Zhou, Sci. Rep. **6**, 18860 (2016).
[14]S.-C. Liu, D. Zhao, Y. Liu, H. Yang, Y. Sun, Z. Ma, C. Reuterskiöld-Hedlund, M. Hammar, and W. Zhou, Appl. Opt. **56**, H67 (2017).
[15]P.-T. Lee, T.-W. Lu, and K.-U. Sio, J. Lightwave Technol. **29**, 1797 (2011).
[16]K. Hirose, Y. Liang, Y. Kurosaka, A. Watanabe, T. Sugiyama, and S. Noda, Nat. Photonics **8**, 406 (2014).
[17]K. Baumann, T. Stöferle, N. Moll, R. F. Mahrt, T. Wahlbrink, J. Bolten, T. Mollenhauer, C. Moormann, and U. Scherf, Appl. Phys. Lett. **91**, 171108 (2007).
[18]S.-L. Chua, Y. Chong, A. D. Stone, M. Soljačić, and J. Bravo-Abad, Opt. Express **19**, 1539 (2011).
[19]J.-H. Choi, Y.-S. No, M.-S. Hwang, S.-Y. Kwon, K.-Y. Jeong, S.-H. Kwon, J.-K. Yang, and H.-G. Park, Appl. Phys. Lett. **104**, 091120 (2014).
[20]J. O. Grepstad, M. M. Greve, B. Holst, I.-R. Johansen, O. Solgaard, and A. Sudbø, Opt. Express **21**, 23640 (2013).
[21]A. Kodigala, T. Lepetit, Q. Gu, B. Bahari, Y. Fainman, and B. Kanté, Nature **541**, 196 (2017).
[22]A. F. Oskooi, D. Roundy, M. Ibanescu, P. Bermel, J. D. Joannopoulos, and S. G. Johnson, Comput. Phys. Commun. **181**, 687 (2010).
[23]M. Barth, J. Kouba, J. Stingl, B. Löchel, and O. Benson, Opt. Express **15**, 17231 (2007).
[24]J. Vučković, M. Lončar, H. Mabuchi, and A. Scherer, IEEE J. Quantum Electron. **38**, 850 (2002).